

Article

RETRACTED: Catalytic Combustion Characteristics of Methane-Air Mixtures in Small-Scale Systems at Elevated Temperatures

Junjie Chen , Xuhui Gao  and Deguang Xu 

Department of Energy and Power Engineering, School of Mechanical and Power Engineering, Henan Polytechnic University, Jiaozuo 454000, China; huitpj@163.com (X.G.); gaotpj@163.com (D.X.)

* Correspondence: comcjj@163.com or cjj@hpu.edu.cn; Tel.: +86-15138057627

Received: 18 September 2018; Accepted: 4 October 2018; Published: 6 October 2018



Abstract: The catalytic combustion characteristics of methane-air mixtures in small-scale systems were investigated at elevated temperatures, with particular emphasis on identifying the main factors that affect formation and removal of combustion-generated pollutants. Computational fluid dynamics simulations were performed using detailed chemical kinetic mechanisms, and more insights were offered into the phenomena occurring in the temperature range where homogeneous and heterogeneous reaction pathways are both important. Reaction engineering analysis was performed to provide an in-depth understanding of how to achieve low emissions of pollutants. Spatial distributions of the major species involved were presented to gain insight into the interplay between the two competing pathways involved. The results indicated that the distribution of oxidized products depends critically on the feed composition, dimension, temperature, and pressure. Small-scale catalytic systems enable low emissions of pollutants even in a high temperature environment, along with high combustion efficiency. The interplay between the two competing pathways via radicals is strong, and the heterogeneous pathway can significantly inhibit the homogeneous pathway. The inhibiting effect also accounts for the low emissions of nitrogen oxides. Almost all of the nitrogen oxides emitted by small-scale catalytic systems are nitric oxide. Catalytic combustion technology can be used to reduce the formation of undesired products, especially pollutant nitrogen oxide gases far below what can be achieved without catalysts. Recommendations for the design of small-scale catalytic systems are provided.

Keywords: combustion characteristics; numerical simulations; catalytic combustion; pollutant formation; small-scale systems; reaction pathways; product distributions; computational fluid dynamics

1. Introduction

Small-scale combustion systems where the combustion process takes place in very small volumes are emerging as a powerful tool for portable production of clean, economical energy [1–4]. These portable energy generation systems will eventually replace conventional lithium-ion batteries due to the high specific energy of hydrocarbon fuels [5,6]. Furthermore, they also provide the opportunity for efficient heat sources for endothermic reactions, such as steam reforming [7,8] and ammonia decomposition [9,10] in miniaturized chemical systems for the production of hydrogen for fuel cell applications. Advances are occurring on all these fronts, but progress is usually achieved on small-scale gas-phase combustion systems [1,2,5,6]. Due to potential increases in future demand for portable energy generation systems with low pollutant emissions, the technical issues associated with small-scale gas-phase combustion technology has been highlighted.

The combustion of fuel can be achieved in two ways [1–4]. The most common is gas-phase combustion, which proceeds at a high temperature and is usually in the presence of a flame [11–14]. As an alternative to gas-phase combustion, catalytic combustion holds great promise for speeding desired oxidation reactions and reducing the formation of undesired products [15–18]. There are many examples of catalytic combustion systems [19–24], and applications are often divided into primary combustion, where the objective is the generation of heat or power for mechanical drive or electric power applications such as fuel cells, modern reciprocating engines, and gas turbines; and secondary applications, where the purpose is the destruction of pollutants. Sometimes an application achieves both purposes in this style of combustion. Efforts to develop this technology focus on improving combustion efficiency and reducing pollutant emissions [21,22,25,26]. However, the careful balance between operating performance and low emissions often requires that the performance of catalytic combustion systems be optimized for specific purposes.

This increased focus on catalytic combustion arises from a variety of advantages this technology offers [5,6]. Gas-phase combustion is usually faster than catalytic combustion, but gas-phase flames are often quenched when confined within spaces with critical sub-millimeter dimensions due to radical and thermal quenching [27,28]. In contrast, catalytic systems can dramatically improve the stability of combustion over what had previously been possible by means of gas-phase systems [29,30]. Additionally, catalytic systems enable complete combustion at lower temperatures than would otherwise be possible, thereby avoiding the formation of nitrogen oxides and leading to controllable catalytic reactions [31,32]. These features can offer multiple benefits during combustion, such as near zero nitrogen oxides emissions while minimizing combustion instability [5,6]. Small-scale systems enable very high transport rates, which confirms the potential of catalytic combustion technology [33,34]. Furthermore, catalytic combustion systems enable fast start-up and transient response [35,36], and can be designed with very simple geometry, which can greatly simplify design and reduce cost [37,38]. In summary, catalytic combustion systems offer major performance benefits and design advantages, such as reduced combustion instability, lower peak temperatures, leaner combustion, lower emissions, and simplified design, when compared to conventional state of the art gas-phase combustion systems.

The need for catalytic devices in the control of pollution has been firmly established for many years. The emergence of catalytic combustion strategies offers the potential to greatly reduce emissions of pollutants with minimal aftertreatment and to significantly improve operating efficiency, thus holding great promise in a wide variety of applications [39,40]. Design of efficient reliable systems requires an understanding of the basic operating principles of these small-scale catalytic devices [5,6,41,42]. Knowledge of the characteristics of combustion in small-scale catalytic systems is of great importance and allows insight into the formation of pollutants. Much effort has been devoted to improve the understanding of mechanisms of the formation of pollutants in these systems and to develop control strategies to reduce their emissions [3,4,21,22]. There are reports claiming that the emissions of pollutants can be substantially reduced by means of catalytic combustion, even in a high temperature environment [43,44]. Despite all the recent advances in description and understanding in this regard, there are quite a few aspects of combustion characteristics in need of further research. These include the role of heterogeneous and homogeneous pathways in determining the distribution of products, identification of the major factors controlling the emissions of pollutants, and description of different combustion processes.

This research focuses on the combustion characteristics in small-scale catalytic systems at elevated temperatures, at which heterogeneous and homogeneous reactions can occur simultaneously [1,2,5,6]. The behavior of small-scale catalytic systems under these conditions may be of interest in terms of potential application to high temperature catalytic processes. For example, much attention has been focused on catalytic combustion of lean fuel-air mixtures in gas turbines as a means of achieving low emissions of pollutants [21,22]. Small-scale catalytic combustion systems benefits also from the homogeneous reaction which increases the overall efficiency [1,2,5,6].

In the present study, a two-dimensional numerical model that incorporate detailed reaction mechanisms was developed to better understand the role of heterogeneous and homogeneous pathways in determining the distribution of combustion-generated products. Computational fluid dynamics simulations were carried out to optimize operating conditions and to gain understanding of the reaction pathways involved in the catalytic combustion process occurring in a high temperature environment. The objective of the present study is to understand how catalytic combustion aids in reducing pollutant emissions from small-scale systems at elevated temperatures. Special emphasis is placed on understanding the role of various reaction pathways in determining the distribution of combustion-generated products.

2. Physical System and Modeling Approach

Numerical simulations [45–50], in conjunction with experiments [51,52], have played an important role in catalytic combustion technology by providing analysis of specific systems, and subsequently the evaluation of potential performance advantages relative to conventional gas-phase combustion systems. Computer simulations are assisting in design and optimization of small-scale catalytic combustion systems, thereby providing important and unique insights into the nature of combustion itself [53,54].

2.1. Physical Description of the Small-scale System

The concept of CATHLEAN hybrid catalytic combustion systems [21,40] has been proposed to improve the operating conditions required for existing gas turbine combustors, thereby greatly reducing the technical risk associated with their commercial applications. This approach addresses the difficulties in developing advanced, ultra-low NO_x , hybrid combustion technology required for the design of gas turbine combustors with a catalytic component [21,40]. A schematic diagram of the CATHLEAN hybrid catalytic combustion system with its crucial components is depicted in Figure 1. The system is designed primarily to achieve ultra-low NO_x emissions from catalytic natural gas combustion for the intended application [21,40]. The design of the CATHLEAN hybrid catalytic combustion system is illustrated in Figure 2. Further details about the combustion system designed for specific applications such as full-scale atmospheric testing are available in the literature [21,40]. One of the main features of the combustion system is the multifunctionality of the catalytic reactor. In a typical catalytic reactor, the gas flows through parallel, multiple sub-millimeter channels with a catalyst located on their walls in a porous washcoat, where it is effective to tight control the reaction pathways involved in the chemical process [5,6]. In order to better understand the behavior of these catalytic reactors, there is a parallel need for reliable computational fluid dynamics models to help predict the characteristics of catalytic combustion in small-scale systems. The present work is centered around modeling a single channel of the catalytic reactor. It is assumed that the distribution of flow velocity in each of the channels in the catalytic reactor is uniform and that all channels behave in a similar manner when modeling only a single channel.

The small-scale combustion system to be modeled is a single-channel catalytic reactor with a premixing method to form a lean methane-air mixture for combustion. The catalytic reactor consists of two parallel plates of length 8.0 mm and thickness 0.2 mm, separated by a gap distance 0.8 mm between them, unless otherwise specified. A schematic diagram of the small-scale catalytic combustion system is illustrated in Figure 3. The fuel used for the combustion system is methane, which is chosen as a representative of natural gas. A platinum-based catalyst is used for catalytic oxidation of the fuel, since there is an established knowledge base related to chemical kinetics over this catalyst, and this catalytic process offers the advantages of ready availability of chemical kinetic models. The walls of the reactor are coated with a washcoat containing the catalyst. Combustion-generated pollutants, such as nitrogen oxides, carbon monoxide, and unburned hydrocarbons, inside the catalyst washcoat could be further converted to nitrogen gas, carbon dioxide, and water vapor [21,22,43,44].

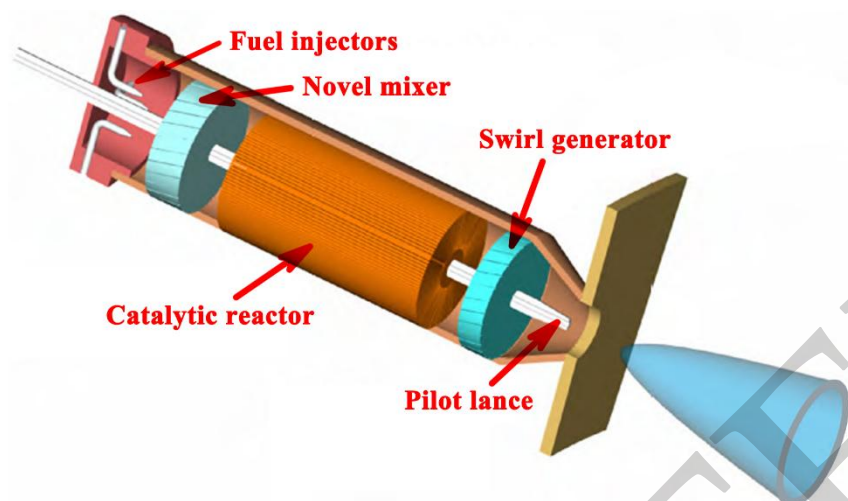


Figure 1. Illustration of the CATHLEAN hybrid catalytic combustion system with its crucial components.

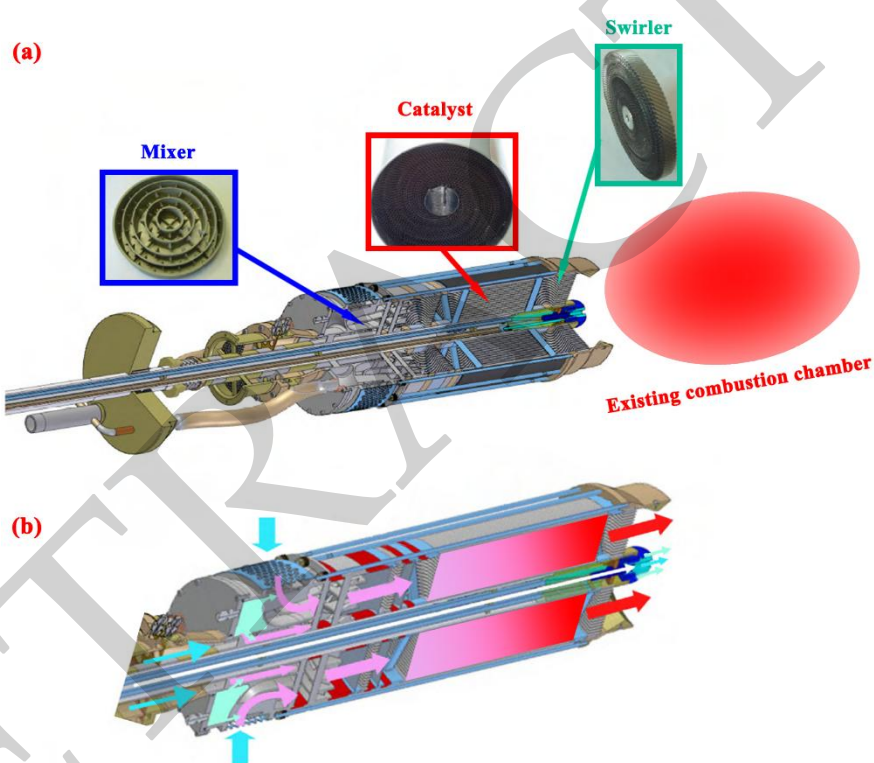


Figure 2. (a) Example of a CATHLEAN hybrid catalytic combustion system with its crucial components. (b) Design of the CATHLEAN hybrid catalytic combustion system, with arrows indicating the direction of flow.

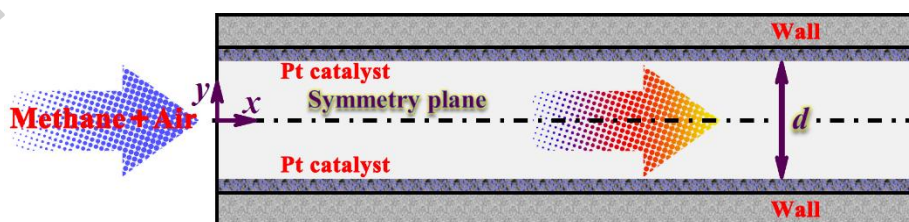


Figure 3. Schematic representation of the small-scale catalytic combustion system. Arrows indicate the direction of flow. Fuel and air are evenly premixed upstream of the system, thereby enabling the system to achieve optimal overall performance.

A set of standard values are chosen for the various design parameters in the model being developed, and then one of the parameters varies. A set of parameters are defined to describe the model being developed, such as reactor dimension (0.3–2.0 mm), wall temperature (1200–2000 K), fuel-to-air equivalence ratio (0.2–1.0), and pressure (0.1–2.0 MPa). The wall temperature is so high that the combustion reaction is limited by transport effects and diffusion plays an overwhelming role in the operation of these systems [1,2,5,6]. By referring to these parameters, the catalytic combustion process under different operating conditions is readily described.

A list of standard values is provided as follows. The small-scale catalytic combustion system consists of a catalytic monolith reactor, as described in detail in the literature [55]. Monolith reactors offer the advantage of good mass transfer performance, high surface-area-to-volume ratio, thinner walls, ease of product separation, and low pressure drop [56,57]. The single-channel catalytic reactor is 8.0 mm in length. The thickness of each parallel plate is 0.2 mm. The gap distance between two adjacent parallel plates is 0.8 mm. The temperature of the incoming combustible gas mixture is fixed at 300 K, and the inlet and surrounding temperatures are assumed to be equal. The fuel-to-air equivalence ratio of the mixture is taken equal to 0.8, since combustion systems operated under lean conditions are beneficial for the reduction of nitrogen oxides [32]. The flow velocity is set to be 0.8 m/s at the inlet of the reactor. The thermodynamic system is operated at atmospheric pressure. The monolith catalyst consists of platinum deposited on an alumina-coated cordierite substrate. The thickness of the catalyst washcoat is assumed to be 0.08 mm, with a tortuosity factor of 3, a porosity of 0.5, and a mean pore diameter of 20 nm. The total available site density for the platinum catalyst is assumed to be 2.72×10^{-9} mol/cm² [55]. The catalyst washcoat contains 0.16 g alumina per gram of cordierite substrate, with a platinum loading of 0.01 g per gram of substrate. More details about the properties of the catalyst washcoat used in the present study are available in the literature [55], where the synthesis method has been described in detail.

In addition, the nominal wall temperature is taken equal to 1500 K, which often represents a maximum allowable temperature limit for a catalytic reactor. As will be discussed later, the wall temperature is a useful design parameter used to characterize combustion. The choice of the nominal wall temperature defined herein stems from similar temperatures observed in short contact time catalytic reactors, in which noble metal catalysts have been found to be stable up to a temperature of about 1500 K [58,59]. This temperature threshold is usually set as the limit of material stability for small-scale catalytic reaction systems [41,60–63]. Wall and catalyst temperatures in excess of this threshold are deemed detrimental to the catalytic reactor. Modeling the catalytic reactor under extreme conditions (e.g., at 1500 K) is useful to better understand how to achieve low emissions of pollutants from a small-scale catalytic combustion system operated at elevated temperatures where the formation of the oxides of nitrogen becomes more favorable [64,65].

2.2. Mathematical Model

The small dimension of the combustion system implies that transport processes are strongly influenced by diffusion. However, the characteristic length scale is still sufficiently large compared to the mean free path for the combustion problem involved. Consequently, classical continuum descriptions are appropriate [66,67]. Additionally, the Reynolds number is found to be less than 680 in all of the cases examined. As a result, the reactive flow in the small-scale catalytic system is laminar.

The model depends on the following assumptions:

- The thermodynamic system operates under steady-state conditions.
- The gaseous mixture is assumed to behave qualitatively as an ideal gas.
- The flow distribution at the inlet of the channel is flat in the transverse direction.
- Pressure drop in the channel is negligible.
- There is a constant gas concentration and temperature at the inlet of the channel.
- The catalyst is uniformly distributed on the surface of the catalytic reactor.

Modeling the chemically reacting system requires the solution of a set of coupled non-linear partial differential equations using an appropriate numerical method. The modeling tool used in the present work is commercial computational fluid dynamics codes ANSYS Fluent [68], which uses the finite volume method to solve the governing system of partial differential equations [69]. The following conservation equations are solved for the gas phase.

The continuity equation ensures conservation of mass in the gas phase:

$$\frac{\partial(\rho u)}{\partial x} + \frac{\partial(\rho v)}{\partial y} = 0 \quad (1)$$

The momentum balance equations solved for the fluid domain are given by

$$\frac{\partial(\rho uu)}{\partial x} + \frac{\partial(\rho vu)}{\partial y} + \frac{\partial p}{\partial x} - \frac{\partial}{\partial x} \left[2\mu \frac{\partial u}{\partial x} - \frac{2}{3}\mu \left(\frac{\partial u}{\partial x} + \frac{\partial v}{\partial y} \right) \right] - \frac{\partial}{\partial y} \left[\mu \left(\frac{\partial u}{\partial y} + \frac{\partial v}{\partial x} \right) \right] = 0 \quad (2)$$

$$\frac{\partial(\rho uv)}{\partial x} + \frac{\partial(\rho vv)}{\partial y} + \frac{\partial p}{\partial y} - \frac{\partial}{\partial x} \left[\mu \left(\frac{\partial v}{\partial x} + \frac{\partial u}{\partial y} \right) \right] - \frac{\partial}{\partial y} \left[2\mu \frac{\partial v}{\partial y} - \frac{2}{3}\mu \left(\frac{\partial u}{\partial x} + \frac{\partial v}{\partial y} \right) \right] = 0 \quad (3)$$

The steady state energy balance equation solved for the fluid domain is given by

$$\frac{\partial(\rho uh)}{\partial x} + \frac{\partial(\rho vh)}{\partial y} + \frac{\partial}{\partial x} \left(\rho \sum_{k=1}^{K_g} Y_k h_k V_{k,x} - \lambda_g \frac{\partial T}{\partial x} \right) + \frac{\partial}{\partial y} \left(\rho \sum_{k=1}^{K_g} Y_k h_k V_{k,y} - \lambda_g \frac{\partial T}{\partial y} \right) = 0 \quad (4)$$

The conservation equation solved for the species involved in the gas phase can be written as

$$\frac{\partial(\rho u Y_k)}{\partial x} + \frac{\partial(\rho v Y_k)}{\partial y} + \frac{\partial}{\partial x} (\rho Y_k V_{k,x}) + \frac{\partial}{\partial y} (\rho Y_k V_{k,y}) - \dot{\omega}_k W_k = 0, \quad k = 1, \dots, K_g \quad (5)$$

The various physical symbols presented in the above equations are defined as follows: ρ represents the mass density of the combustible gas mixture; u and v represent the streamwise and transverse components of the flow velocity of the mixture, respectively; x and y represent the streamwise and transverse spatial coordinates in the system being studied herein, respectively; p , μ , and λ_g denote the pressure, dynamic viscosity, and thermal conductivity of the mixture, respectively; h denotes the specific enthalpy of the mixture; T denotes the absolute temperature; K_g denotes the total number of the gaseous species involved in the system; Y_k , h_k , and W_k denote the mass fraction, specific enthalpy, and relative molecular mass of gaseous species k , respectively; the term $\dot{\omega}_k$ denotes the molar rate of production by all gas-phase chemical reactions involving gaseous species k per unit volume; the terms $V_{k,x}$ and $V_{k,y}$ denote the streamwise and transverse components of the diffusion velocity of gaseous species k respectively; the subscript g denotes gas phase.

The diffusion velocity vector is given by

$$\vec{V}_k = -D_{k,m} \nabla \left[\ln \left(\frac{Y_k \bar{W}}{W_k} \right) \right] + \left[\frac{D_k^T W}{\rho Y_k \bar{W}} \right] \nabla (\ln T) \quad (6)$$

wherein the term $D_{k,m}$ is the diffusivity of gaseous species k in the mixture, \bar{W} is the relative molecular mass of the mixture, D_k^T is the thermal diffusivity of gaseous species k , and the nabla symbol ∇ denotes the differential operator del, i.e., nabla operator.

The ideal gas equation of state is

$$p = \frac{\rho RT}{\bar{W}} \quad (7)$$

where R denotes the ideal gas constant. The caloric equation of state can be written as

$$h_k = h_k^0(T_0) + \int_{T_0}^T c_{p,k} dT \quad (8)$$

where h_k^0 indicates the specific enthalpy of formation of gaseous species k at the specified temperature T_0 , and $c_{p,k}$ indicates the specific heat capacity of gaseous species k at constant pressure.

The equation of surface species coverage can be written as

$$\sigma_m \frac{\dot{s}_m}{\Gamma} = 0 \text{ with } m = K_g + 1, \dots, K_g + K_s \quad (9)$$

in which σ_m denotes the site occupancy of surface species m , the term \dot{s}_m denotes the molar rate of production by all surface chemical reactions involving surface species m per unit area, Γ denotes the density of catalyst surface sites, m denotes the total number of gaseous and surface species involved in the system, K_s denotes the total number of the surface species involved in the system, and the subscript m denotes surface phase. The adsorption rate constant is expressed as

$$k_{ad,k} = \left(\frac{2}{2 - s\theta_{free}} \right) \frac{s}{\Gamma^m} \sqrt{\frac{RT}{2\pi W_k}} \quad (10)$$

where s indicates the sticking coefficient and the term θ_{free} indicates the surface coverage of free sites.

The species boundary condition at each of the gas-catalyst interfaces is described by

$$\left(\rho Y_k V_{k,y} \right)_{interface} + \eta F_{cat/geo} W_k (\dot{s}_k)_{interface} = 0, \quad k = 1, \dots, K_g \quad (11)$$

in which η is the effectiveness factor and $F_{cat/geo}$ is the area factor. The surface area of the catalyst washcoat, $A_{catalytic}$, can be related to its geometric surface area, $A_{geometric}$, by this area factor

$$F_{cat/geo} = \frac{A_{catalytic}}{A_{geometric}} \quad (12)$$

The diffusional limitations inside the catalyst washcoat can be estimated as follows [70,71]:

$$\eta = \frac{\dot{s}_{i,eff}}{\dot{s}_i} = \frac{\tanh(\Phi)}{\Phi} \quad (13)$$

$$\Phi = \delta_{catalyst} \left(\frac{\dot{s}_i \gamma}{D_{i,eff} C_{i,interface}} \right)^{0.5} \quad (14)$$

In the above equation, the term $\dot{s}_{i,eff}$ indicates the effective rate of formation of species i on the surface of the catalyst, Φ indicates the Thiele modulus, δ indicates the thickness of the porous washcoat, and the term $C_{i,interface}$ indicates the concentration of species i at the gas-catalyst interface. The catalytic surface area per unit volume of the porous washcoat, γ , is defined to be

$$\gamma = \frac{F_{cat/geo}}{\delta_{catalyst}} \quad (15)$$

The effective diffusivity of species inside the catalyst washcoat and catalyst porosity and tortuosity give the following functional dependence

$$\frac{1}{D_{i,eff}} = \frac{\tau_p}{\varepsilon_p} \left(\frac{1}{D_{i,molecular}} + \frac{1}{D_{i,Knudsen}} \right) \quad (16)$$

in which τ_p represents the tortuosity factor for diffusion inside the washcoat, ε_p represents the porosity of the washcoat, and the term $D_{i,molecular}$ represents the diffusivity for molecular diffusion of species i in the mixture. The diffusivity for Knudsen diffusion of species i is defined to be

$$D_{i,Knudsen} = \frac{d_{pore}}{3} \sqrt{\frac{8RT}{\pi W_i}} \quad (17)$$

where d_{pore} represents the mean pore diameter.

To completely decouple the kinetic effect from the thermal effect, isothermal surface conditions are considered in the present work, and a fixed wall temperature is imposed on the surface of the catalyst. In the energy balance, the surface boundary is set to constant temperature, so that no heat is lost from the chemically reactive system being studied herein, i.e., the reactor walls are adiabatic.

2.3. Detailed Chemical Kinetic Model

Success in modeling combustion chemistry is dependent upon the reliability of the chemical kinetic model used. Modeling of the small-scale system with detailed reaction mechanisms is necessary [72,73] to accurately describe the catalytic combustion process, and to accurately capture the combustion characteristics such as the formation of pollutant species. The influence of nitrogen in a high temperature environment must also be accounted for. In the present work, homogeneous and heterogeneous reactions are incorporated into the model simultaneously by using detailed mechanisms, and nitrogen chemistry in high-temperature combustion is also included in the chemical kinetic model. Special attention will be given to nitrogen combustion chemistry involved in the homogeneous reaction mechanism used. The homogeneous reaction term is included herein to help with emissions predictions and to allow the model to be as general possible.

Both heterogeneous and homogeneous chemistry were modeled simultaneously to provide an accurate description of the catalytic combustion process being studied herein. The homogeneous reaction mechanism used herein is the Gas Research Institute mechanism describing homogeneous oxidation of methane [74]. The Gas Research Institute mechanism is one of the first mechanisms freely available on the internet describing methane oxidation kinetics with NO_x chemistry to help with emissions predictions [75]. This high-temperature methane oxidation mechanism contains the elementary reactions involved with nitrogen, and has been tested more thoroughly than any other mechanism in combustion history. For example, this mechanism contains detailed steps involved during prompt NO_x formation and reburn [74]. With nitrogen added to the system in a combustion environment, the chemical kinetics occurring in the gas phase are considerably more complex.

The detailed chemical kinetics of methane oxidation on supported platinum developed by Deutschmann and co-workers [55] are used in the chemical kinetic model as the heterogeneous reaction mechanism. The full heterogeneous mechanism is freely available on the internet. The homogeneous and heterogeneous reaction mechanisms are incorporated into the code using the Sandia CHEMKIN [76] and Surface-CHEMKIN [77], respectively. All of the mechanisms used are presented in a format compatible to CHEMKIN codes. The thermodynamic properties for the species involved in the model are adopted from the chemical kinetic mechanisms given above. The Sandia CHEMKIN [76] and Surface-CHEMKIN [77] subroutine packages are then integrated into the ANSYS Fluent codes [78,79] to solve the two-dimensional conservation equations given above.

2.4. Computation Scheme

For the combustion problem involved, all physical properties of the mixture of methane and air are taken to be dependent on the local temperature and composition. The temperature of the incoming gas is assumed to be constant, although it is more likely that diffusion effects will heat the gas before it arrives at the entrance to the reactor. The density of the mixture is evaluated using the ideal gas law. Transport properties of all of the species involved in the system are included in the model. The boundary condition for the momentum balance is a no-slip condition at each of the gas-catalyst interfaces. The chemically reacting system is nonlinear inherently due to the exponential dependence of the rate of the combustion reaction on temperature. An orthogonal staggered grid is used, with grid points clustered in the region near the surface of the catalyst to capture the velocity and temperature gradients more accurately. The grid consists of 200 nodes in the axial direction and 80 nodes in the transverse direction for the nominal reactor dimension. Furthermore, to control the discretization error, more grid points are placed in regions in which the solution is changing rapidly. In this context, the solution is accurate in the vicinity of these regions, and the resolution of the grid used is sufficient to produce properly converged results. The solution is deemed converged when the residuals of the conservation equations given above are less than 10^{-6} .

Convergence of the mathematical solution is usually difficult to solve strongly nonlinear, stiff differential equations of coupled chemical kinetics. The solution usually takes at least several hours or even days to converge due to the large number of the above-listed nonlinear governing equations, as well as the complexity of the individual elementary reactions involved in the detailed chemical kinetic model, i.e., the stiffness problem in chemical kinetics. An example of the residuals for the conservation equations during the course of the mathematical solution is shown in Figure 4. The iteration continues until the correction computed for the next iterate is sufficiently small, as defined above. The plot indicates that the convergence criterion is satisfied after about 800 iterations.

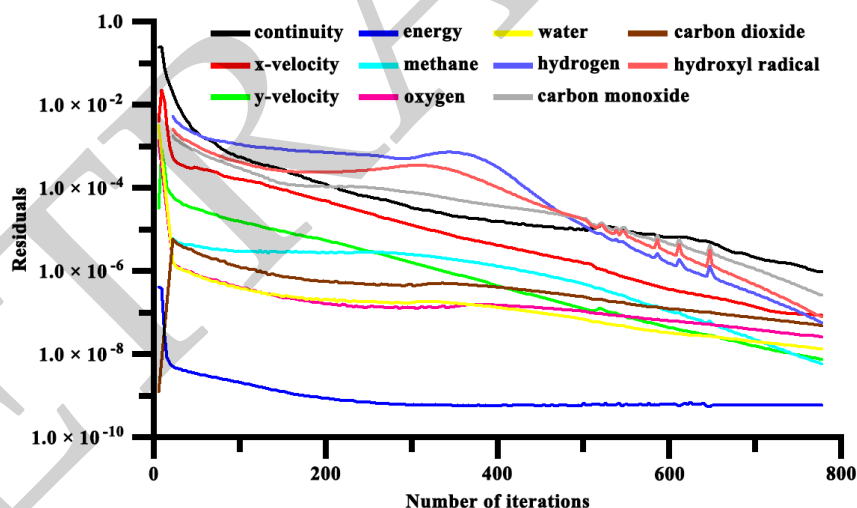


Figure 4. Example of residuals for the conservation equations during the course of the solution. The mesh used here consists of 16,000 nodes in total. All parameters are set to standard values.

2.5. Numerical Validation

In order to verify the numerical scheme implemented in the present work, the experimental and numerical results obtained by Dogwiler et al. [78] are utilized. A quantitative comparison of model predictions with experimentally measured relevant quantities is made for a small-scale catalytic combustion system with three different fuel-air equivalence ratios, denoted as cases (A), (B), and (C), over a wide range of operating conditions. Details of these test cases are available in the literature [78]. The same experimental parameters are used in the analysis of the results obtained from the model. The distribution of the catalyst temperature field measured by means of thermocouples

serves as the energy boundary condition at each of the gas-catalyst interfaces. The axial hydroxyl radical concentration profiles predicted and measured along the fluid centerline after the position of homogeneous ignition are shown in Figure 5. The sudden rise in the hydroxyl radical concentration along the fluid centerline represents the initiation of homogeneous reactions. The predicted and measured hydroxyl radical concentration distributions are found to be in good agreement and within the limits of measurement error and experimental repeatability. Therefore, the model accurately predicts the trend in the experimental data. The overall agreement between model predictions and experimental measurements shows that modeling can serve as a reliable design tool in examining catalytic combustion characteristics under conditions that are not easily reproduced experimentally.

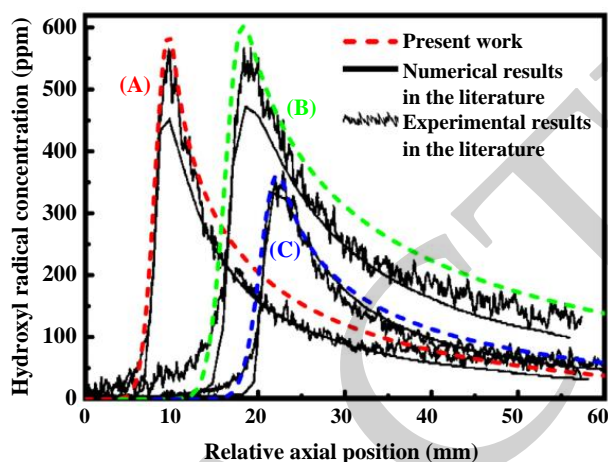


Figure 5. Axial hydroxyl radical concentration profiles predicted and measured along the fluid centerline after the position of homogeneous ignition. The operating conditions of the small-scale catalytic combustion system are given as follows: case (A), $\varphi = 0.37$, $u_{in} = 1.0$ m/s, $T_{in} = 750$ K, case (B), $\varphi = 0.37$, $u_{in} = 2.0$ m/s, $T_{in} = 729$ K, and case (C), $\varphi = 0.31$, $u_{in} = 1.0$ m/s, $T_{in} = 754$ K, where φ is the fuel-air equivalence ratio, u_{in} is the inlet velocity, and T_{in} is the inlet temperature.

3. Combustion Modes and Major Pollutants

3.1. Combustion Modes

Combustion can occur in different modes. To gain insight into the competing reaction pathways involved in catalytic combustion, computational fluid dynamics simulations are performed for three different modes of combustion. In the coupled homogeneous–heterogeneous combustion mode [79,80], both gas-phase and surface reactions can occur simultaneously, and homogeneous and heterogeneous pathways are both important. The purely heterogeneous combustion mode only takes the reactions occurring on the surface of the catalyst into account by setting the rate of the homogeneous reaction equal to zero [81,82]; the homogeneous pathway is of no consequence in this regard. This idealized combustion mode cannot be used in general except under conditions where the rate of homogeneous reactions is much lower than that of heterogeneous reactions. The idealized purely heterogeneous combustion mode is a limiting case of the coupled homogeneous–heterogeneous combustion mode. In the purely homogeneous combustion mode, combustion can occur only in a flame mode [83,84]. In this combustion mode, the surface of the reactor is chemically inert and only the reactions occurring in the gas phase are taken into account by setting the rate of the heterogeneous reaction equal to zero [81,82]. The homogeneous pathway is important, and the catalytic reactor becomes functionally equivalent to a gas-phase combustion system in this regard. A detailed comparison between the results obtained by these modes is made, and the difference between these modes of combustion is illustrated in the following sections.

3.2. Major Pollutants

On the other hand, there are three major pollutant species routinely considered in energy generation from combustion: nitrogen oxides, carbon monoxide, and unburned hydrocarbons [85,86]. It is important to emphasize that the term “nitrogen oxides”, collectively termed NO_x , refers specifically to the combination of nitric oxide and nitrogen dioxide. Nitrogen oxides are formed by oxidation of nitrogen in the gas phase. One of the major motivations for the development of small-scale catalytic combustion systems is to reduce the emissions of nitrogen oxides [1,2,5,6]. Carbon monoxide is the product of incomplete combustion, and can be further oxidized to carbon dioxide. A considerable portion of the discussion presented herein will focus on reducing the emissions of nitrogen oxides, because the effort to reduce the emissions of pollutants has dominated the development of catalytic combustion technology [32]. A detailed discussion on the results obtained for these major pollutants are also presented in the following sections.

Hereafter, it is assumed that all parameters other than those displayed are kept at their standard values, as stated previously.

4. Results

4.1. Coupled Homogeneous-Heterogeneous Combustion Characteristics

In the coupled combustion mode, the resulting spatial distributions of gas temperature, fuel conversion, and major species in the catalytic reactor operated at atmospheric pressure are shown in Figure 6. The rise of gas temperature is quite high along the direction parallel to the flow (Figure 6a). This feature is representative of the microreactor being used for catalytic combustion. The very rapid temperature rise leads to the autoignition of the fuel in the reactor with a constant wall temperature. As a result, the fuel is consumed rapidly near the entrance to the system, and complete conversion of the fuel is achieved (Figure 6a,b), indicating that most of the combustion reaction takes place in the front part of the catalytic reactor. Carbon monoxide is usually formed from the oxidation of methane in the gas phase under oxygen-deficient conditions. Under oxygen-rich conditions, the fuel is partially oxidized to carbon monoxide near the entrance to the reactor, but the concentration of this partial combustion product falls very rapidly to a rather insignificant magnitude along the direction parallel to the flow (Figure 6c). This is because carbon monoxide is rapidly oxidized in the gas phase to carbon dioxide by reaction with excess oxygen.

On the other hand, the amount of the nitric oxide formed within the catalytic reactor is very low, and then this product is removed from the gas phase until the outlet of the reactor (Figure 6d). In this combustion mode, nitric oxide is formed and removed continuously in the catalytic reactor, but it is interesting to note that its final concentration is insignificant. With the rise of gas temperature, smaller radical species with higher concentrations are formed, eventually leading to autoignition of the fuel in the gas phase. Transport of these radical species is important for the combustion reaction occurring in the gas phase. For example, the mass fraction of hydroxyl radical reaches a peak just before the complete conversion of the fuel involved in the combustion in this mode (Figure 6e).

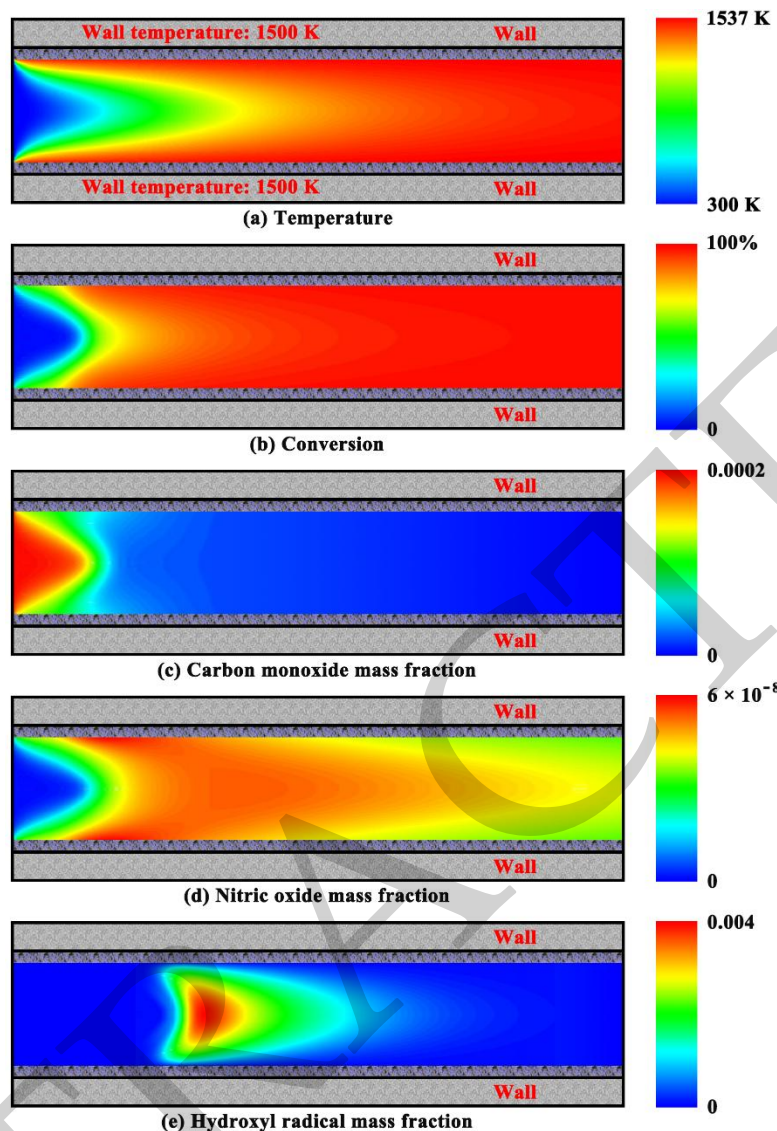


Figure 6. Contour plots of gas temperature, fuel conversion, and major species concentration at atmospheric pressure obtained for the reactor described in terms of the coupled combustion mode, keeping a fixed wall temperature of 1500 K. (a) Gas temperature; (b) Fuel conversion; (c) Carbon monoxide concentration; (d) Nitric oxide concentration; (e) Hydroxyl radical concentration. All parameters are set to standard values.

4.2. Purely Heterogeneous Combustion Characteristics

In the purely heterogeneous mode, the contour plots of gas temperature, fuel conversion, and major species concentration in the reactor operated at atmospheric pressure are shown in Figure 7. The reaction occurs rapidly, and its rate remains nearly constant before the reaction proceeds to completion (Figure 7b). Mass-transfer limitations are found within the fluid region. The combustion reaction occurring on the surface of the catalyst can be approximated as first-order, since it is limited by transport effects which are proportional to the partial pressure of the fuel being burnt with a catalyst. On the other hand, carbon monoxide is formed very rapidly within the reactor with a constant wall temperature, but then is gradually converted to carbon dioxide (Figure 7c). Consequently, the amount of carbon monoxide formed is insignificant at the outlet of the reactor. The concentration of the fuel being burnt with a catalyst continues to decrease (Figure 7d), whereas the concentration of the carbon dioxide formed during combustion continues to increase (Figure 7e). The heterogeneous reaction is so rapid that the concentration of the fuel in the vicinity of the catalytic walls is nearly zero, and

diffusion of the fuel to the surface of the catalyst is rate limiting (Figure 7d). There is no formation of nitrogen compounds, because the nitrogen chemistry is dominated by homogeneous pathways. In this combustion mode, the concentration of hydroxyl radicals in the gas phase is very low (Figure 7f). On the other hand, there exists steep gradients in temperature and species within the small-scale system, as shown in Figure 7.

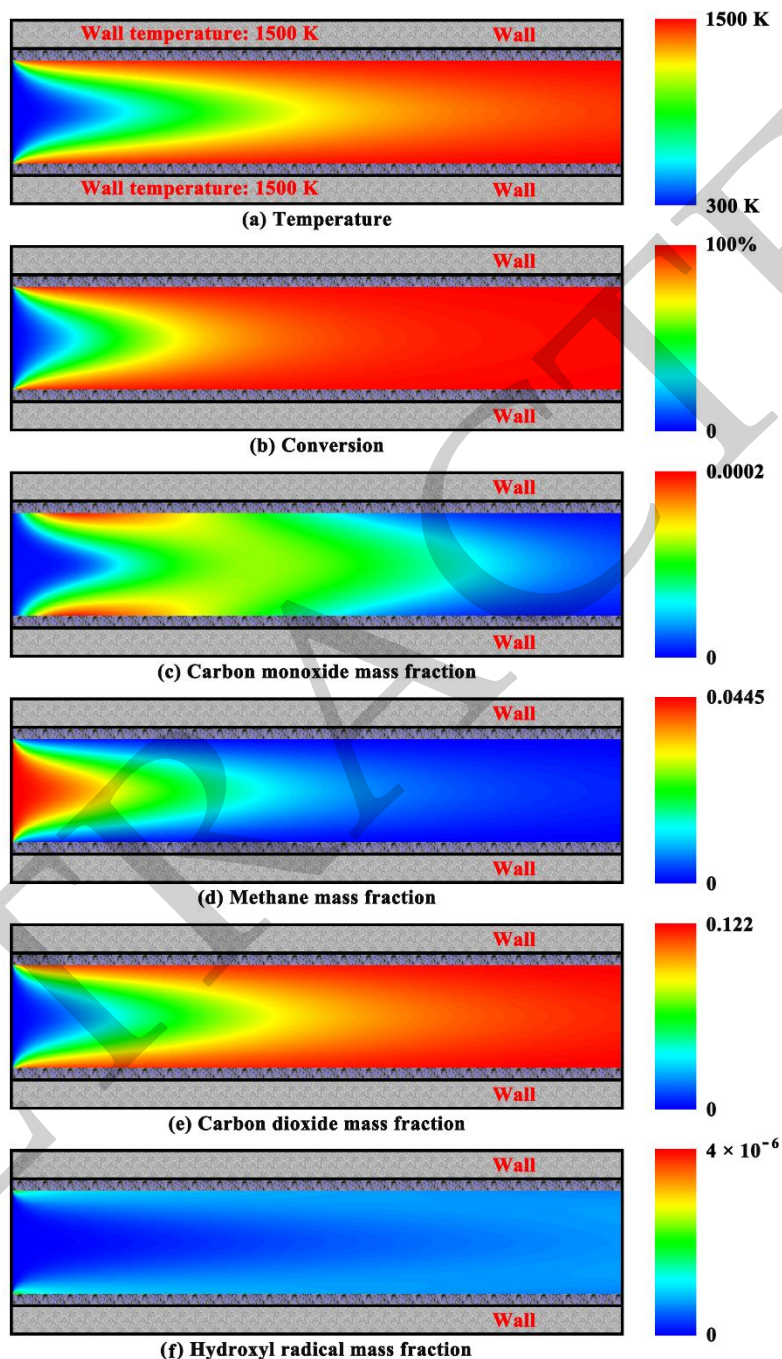


Figure 7. Contour plots of gas temperature, fuel conversion, and major species concentration at atmospheric pressure predicted by the purely heterogeneous combustion mode, keeping a fixed wall temperature of 1500 K. (a) Gas temperature; (b) Fuel conversion; (c) Carbon monoxide concentration; (d) Methane concentration; (e) Carbon dioxide concentration; (f) Hydroxyl radical concentration. All parameters are set to standard values.

4.3. Purely Homogeneous Combustion Characteristics

In the purely homogeneous mode, the resulting spatial distributions of gas temperature, fuel conversion, and major species in the reactor with chemically inert walls operated at atmospheric pressure are shown in Figure 8. In the absence of any catalyst, the hot, chemically inert walls of the reactor serve only as an ignition source for the premixed, combustible gas mixture, and a stable flame is physically anchored in the reactor (Figure 8a). The flame temperature, which is determined by a balance of energy between products and reactants, is far below the maximum adiabatic flame temperature obtained from the stoichiometric value for a mixture of methane and air. The flame will be blown-off if the laminar flame speed is too slow compared to the gas flow velocity. At the other extreme, the flame will propagate into the approach flow associated with flashback phenomena if the laminar flame speed is fast relative to the gas flow velocity. Fortunately, catalytic combustion can avoid flashback problems associated with other approaches to combustion [32]. At sufficiently high wall temperatures such as 1500 K discussed herein, the homogeneous combustion reaction can occur spontaneously throughout the premixed mixture in the vicinity of the chemically inert walls even for the relatively low inlet temperature of the mixture (Figure 8a,b).

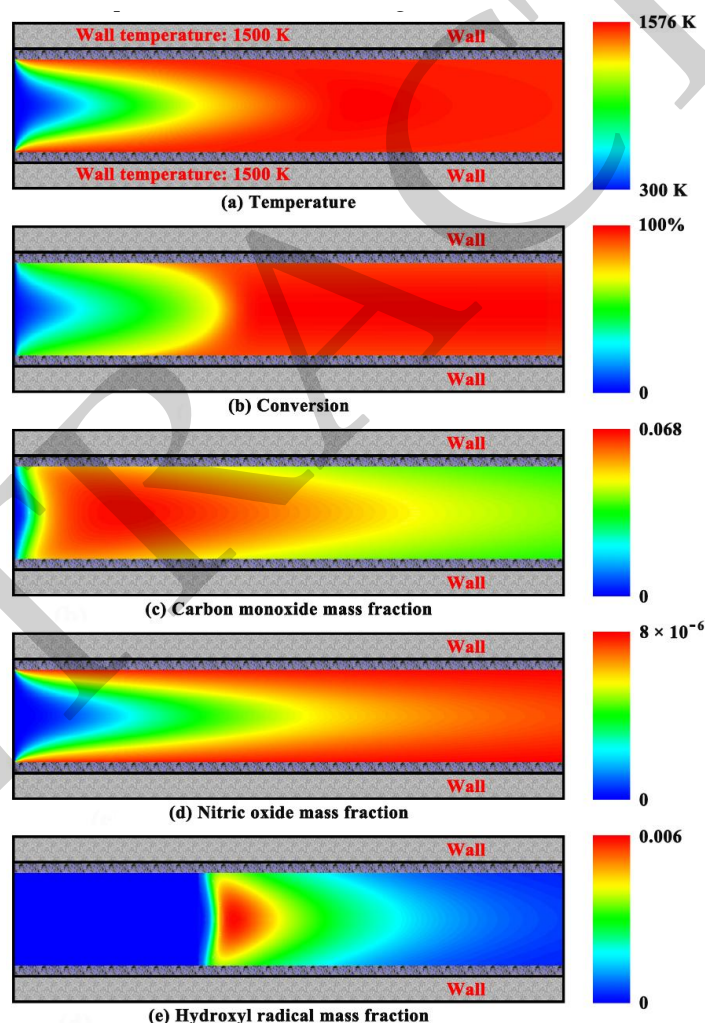


Figure 8. Contour plots of gas temperature, fuel conversion, and major species concentration at atmospheric pressure, predicted by the purely homogeneous combustion mode, keeping a fixed wall temperature of 1500 K. (a) Gas temperature; (b) Fuel conversion; (c) Carbon monoxide concentration; (d) Nitric oxide concentration; (e) Hydroxyl radical concentration. All parameters are set to standard values. The contour plot of hydroxyl radical concentration indicates the location of a premixed flame.

The homogeneous combustion reaction occurs very slowly near the entrance to the reactor with the constant wall temperature, but then proceeds rapidly due to the exponential effect of the gas temperature on the rate of the homogeneous reaction, releasing heat (Figure 8b). In addition, complete conversion of the fuel is possible in a very small region (Figure 8b). Interestingly, rapid gas-phase combustion reactions can be easily sustained in the reactor with chemically inert walls. However, there is an ignition delay for the fuel, the time taken for initiating spontaneous combustion [48], because radical species must be accumulated in the gas phase prior to the start of combustion [87,88]. The fuel is oxidized rapidly, forming a considerable amount of carbon monoxide in the gas phase under the conditions studied herein (Figure 8c). Carbon monoxide subsequently reacts with oxygen to form carbon dioxide. However, there is still a small amount of carbon monoxide that “slips” through the reactor, eventually leading to the emission of this pollutant. There are virtually no nitrogen oxides formed in the gas phase before complete conversion of the fuel involved in the combustion in this mode (Figure 8d). Then, there is a significant increase in the amount of the nitric oxide formed during combustion in the reactor with chemically inert walls. An interesting intermediate species is hydroxyl radicals which are formed in the high-temperature gas-phase region (Figure 8e).

4.4. Effect of Feed Composition

In the coupled combustion mode, the methane conversion and combustion-generated pollutant concentrations obtained in a constant pressure environment are plotted in Figure 9 for different methane-air equivalence ratios. The feed composition plays an appreciable role in reducing the emissions of pollutants from the catalytic reactor. The most important feature shown in the figure is that complete conversion of the fuel can be achieved in all cases except the very lean and near-stoichiometric mixtures. The combustion reaction is extinguished on the surface of the catalyst under sufficiently lean conditions, known as the weak limits. Interestingly, the distribution of combustion-generated pollutants depends on the composition of the feed. The amount of carbon monoxide formed during combustion for various fuel-lean mixtures is considerable within the catalytic reactor used for pollution control, and increases with an increasing equivalence ratio.

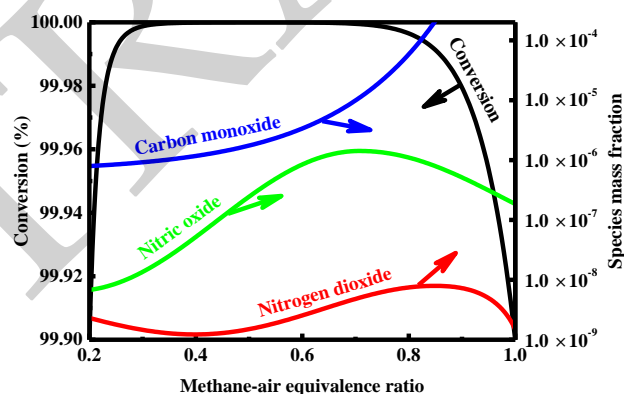


Figure 9. Methane conversion and combustion-generated pollutant concentrations at a constant pressure of 0.5 MPa at different fuel–air equivalence ratios. The pressure is held constant. All parameters are set to standard values except the pressure and the equivalence ratio.

On the other hand, as the equivalence ratio is increased, the concentration of nitric oxide formed in the reactor increases, as shown in Figure 9. However, as the equivalence ratio is increased further after a certain level, the methane conversion drops off, and the amount of nitric oxide formed decreases slightly. The concentration of the nitrogen dioxide formed in a high temperature environment is very sensitive to the composition of the feed. When the equivalence ratio increases, the amount of nitrogen dioxide formed within the catalytic reactor first decreases, then increases, and finally drops off quickly, as shown in Figure 9. Overall, low emissions of nitrogen oxides can be achieved in the catalytic reactor operated under very lean conditions.

4.5. Effect of Dimension

Since the dimension of a chemically reacting system will play an overwhelming role in determining the characteristics of combustion [89,90], the effect of the reactor dimension on catalytic combustion characteristics is evaluated herein for a constant flow velocity.

Figure 10 shows the methane conversion and major species concentrations predicted for the catalytic reactor with different dimensions operated in a constant pressure environment. The conversion results obtained for the reactor with the maximum dimension examined herein (2.0 mm) are similar to those obtained for the reactor described in terms of the purely homogeneous combustion mode shown in Figure 8b, while the conversion results obtained for the reactor with the minimum dimension examined herein (0.3 mm) are similar to those obtained for the reactor described in terms of the purely heterogeneous combustion mode shown in Figure 7b. The peak radical concentration predicted in the catalytic reactor with the maximum dimension appears later, but is still far higher than that predicted in the catalytic reactor with the minimum dimension (Figure 10a). There exists a maximum in the concentration of the carbon monoxide formed in the catalytic reactor with the maximum dimension (Figure 10b). Additionally, the amount of pollutants formed within the catalytic reactor decreases with a decreasing reactor dimension over the entire dimension range examined, but does not change significantly under the conditions studied herein.

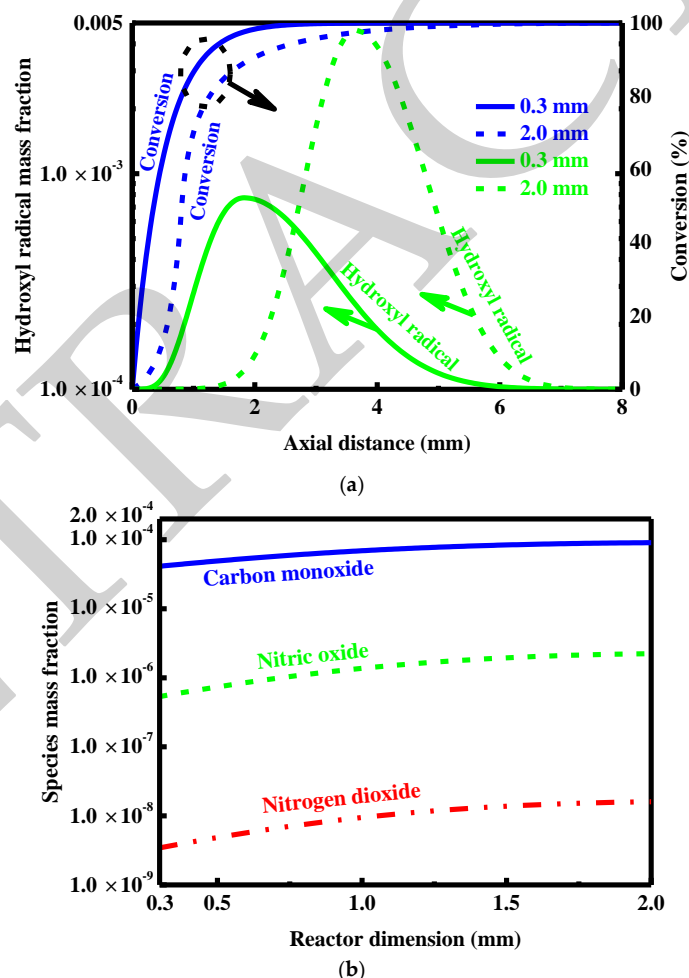


Figure 10. Effect of reactor dimension on the methane conversion and major species concentrations at a constant pressure of 0.5 MPa. (a) Conversion and hydroxyl radical concentration; (b) Nitrogen oxides and carbon monoxide concentrations. All parameters are set to standard values except the pressure and the reactor dimension.

A quantitative comparison of the maximum carbon monoxide concentration is made between different combustion modes. The results shown in Figures 6c, 7c and 8c indicate that the primary pathway of the formation of carbon monoxide within the small-scale combustion system is homogeneous for the nominal reactor dimension. In contrast, the contribution of carbon monoxide formed through a heterogeneous pathway is very small. As the reactor dimension increases, homogeneous reactions become more significant due to the decreased surface-area-to-volume ratio and the reduced mass transfer performance. Therefore, the formation of carbon monoxide becomes more favorable with increasing the reactor dimension, as shown in Figure 10b. The amount of carbon monoxide within the catalytic reactor with the maximum dimension is considerable. However, the concentration of this partial combustion product falls very rapidly to a rather insignificant magnitude along the direction parallel to the flow due to its rapid oxidation reaction with excess oxygen in the gas phase (data not shown), which is consistent with that obtained from the catalytic reactor with the nominal dimension as shown in Figure 6c.

4.6. Effect of Wall Temperature

In the coupled combustion mode, the fuel conversion and combustion-generated pollutant concentrations obtained in a constant pressure environment are plotted in Figure 11 for different wall temperatures. The present results indicate that the conversion of the fuel increases with increasing wall temperature. As expected, the rate of the reaction occurring in the catalytic reactor increases with increasing wall temperature, but the reaction is still approximately first-order. The amount of nitric oxide formed during catalytic combustion increases with increasing wall temperature, as shown in Figure 11. As the wall temperature increases, the amount of nitrogen dioxide formed during catalytic combustion first increases rapidly, then decreases, and finally increases slightly; the amount of carbon monoxide formed within the catalytic reactor falls rather rapidly, and then increases quickly. For a moderate range of wall temperatures, the amount of carbon monoxide formed during catalytic combustion is relatively small, but is one to two orders of magnitude larger than that of the nitrogen oxides formed within the catalytic reactor used for pollution control, as shown in Figure 11.

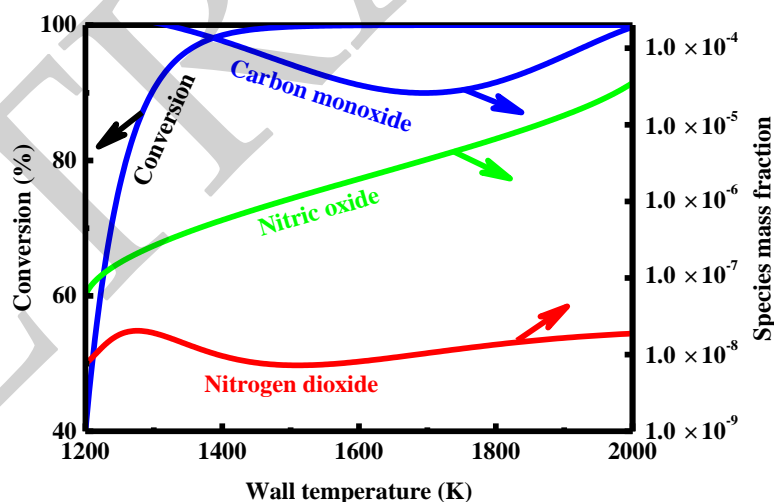


Figure 11. Methane conversion and pollutant concentrations at a constant pressure of 0.5 MPa at different wall temperatures. All parameters are set to standard values except the pressure and the wall temperature.

4.7. Effect of Pressure

The combustion reaction is pressure dependent. The rate of the homogeneous reaction tends to be proportional to the pressure squared [91,92]. In contrast, the rate of the heterogeneous reaction often changes linearly with pressure [93,94]. As a consequence, the contribution to fuel oxidation from heterogeneous pathways increases with increasing pressure. Figure 12 depicts the methane conversion profiles computed at a constant inlet velocity 0.8 m/s when the pressure is variable. The conversion profile shows a gradual change over the entire pressure range considered. The reaction is approximately first-order within the catalytic reactor at elevated temperatures. However, the conversion profile is slightly concave up, especially at high pressures, which is consistent with the ignition delay for the fuel predicted for the reactor described in terms of the purely homogeneous combustion mode. As a result, the reaction occurring in the gas phase becomes more important under high pressure conditions. In this context, there is a large amount of free radical species built up in the gas phase, thereby increasing the contribution to the oxidation of the fuel from homogeneous pathways. On the other hand, pressure has little effect on the effective thermal conductivity of the mixture under the conditions studied herein. In this context, efficient transfer of the heat released in the gas phase by additional homogeneous reactions to the surface of the catalyst is impossible, thereby increasing the potential for homogeneous reactions. The rate of the overall combustion reaction increases with increasing pressure, since high pressures allow faster conversion of the fuel in the catalytic reactor, as confirmed by the conversion curve slope shown in Figure 12.

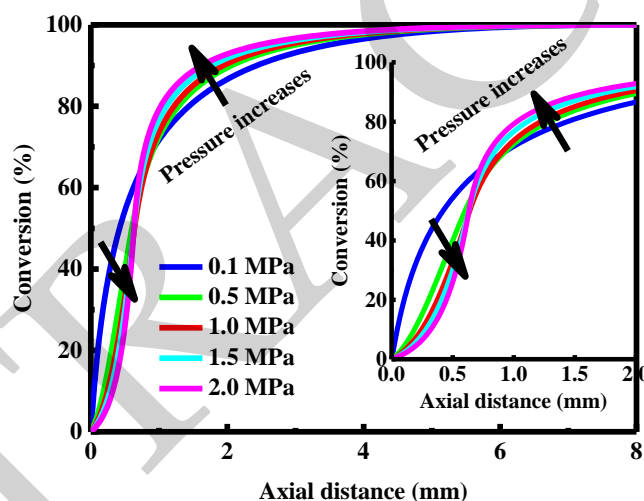


Figure 12. Methane conversion profiles for different pressures. All parameters are set to standard values except the pressure.

Figure 13 shows the pollutant concentrations predicted for the catalytic reactor with different wall temperatures as the pressure is varied. The amount of nitric oxide formed during catalytic combustion increases with increasing pressure. Interestingly, this increase, however, is still far less than that predicted for the reactor operated in the purely homogeneous combustion mode. As the wall temperature is increased from 1500 to 1700 K, the amount of nitric oxide formed within the catalytic reactor increases, with a gradually weakened trend. This result suggests that high operating temperatures tend to promote the formation of nitrogen oxides within the catalytic reactor. The trend observed for the concentration of nitrogen dioxide gives further evidence of this promoting effect. On the other hand, the concentration of the carbon monoxide formed during catalytic combustion of the fuel indicates that high pressures tend to inhibit the formation of carbon monoxide, as illustrated in Figure 13. Overall, the small-scale catalytic system operated at high pressures produces fairly high emissions of pollutants, especially for high operating temperatures.

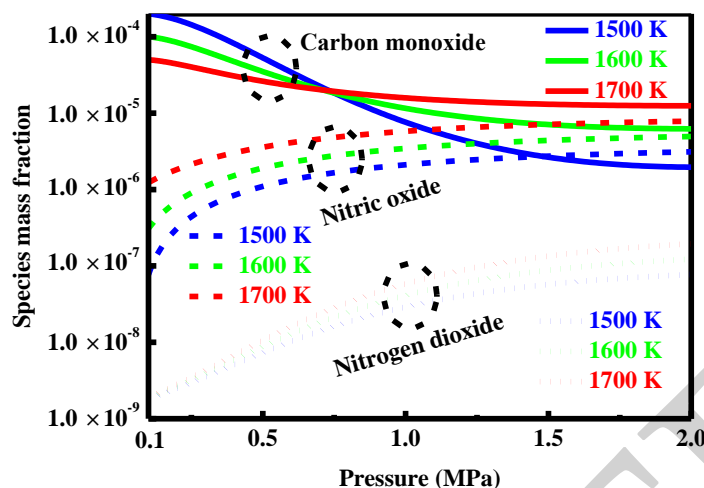


Figure 13. Effect of wall temperature on the concentrations of combustion-generated pollutants at different pressures. All parameters are set to standard values except the pressure and the wall temperature.

5. Discussion

5.1. Competing Pathways of Two Parallel Reactions

Gas temperatures and major species concentrations in the reactor with constant wall temperature have been numerically mapped in two dimensions in Figures 6–8. In this section, various aspects of the reaction pathways involved will be discussed in depth to gain understanding of underlying physicochemical processes. At the temperatures examined herein, both heterogeneous and homogeneous reactions can occur in the catalytic reactor, simultaneously, for the fuel being burnt with or without a catalyst. The results shown in Figures 7 and 8 indicate that each of the reaction mechanisms has its respective significant features of how combustion occurs in a microreactor with a constant wall temperature. Spatial distributions of the major species involved in the system for the three combustion modes examined herein are essentially quite different from each other (Figures 6–8), which is one of the most important features to distinguish different reaction pathways. As discussed earlier, there exists an induction period obtained for the reactor described in terms of the purely homogeneous combustion mode. In contrast, the results obtained for the reactor described in terms of the purely heterogeneous combustion mode are very similar to those obtained from the catalytic combustion process described by first-order chemical kinetics. These differences could potentially be used to distinguish the type of reaction occurring in a chemically reacting system. The relative importance of each reaction pathway can be determined by examining the amount of the species formed homogeneously in the gas phase.

The results shown in Figures 6 and 7 indicate that in the combustion environment being studied, the methane conversion predicted in the reactor operated in the coupled combustion mode is basically similar to that predicted in the reactor operated in the purely heterogeneous combustion mode. The difference in conversion between the two modes of combustion is minor for the reactor with the constant wall temperature. In this case, heterogeneous pathways are predominant in the catalytic combustion process that occurred in the reactor, as confirmed by the smaller amount of nitric oxide that formed in the reactor operated in the coupled combustion mode (Figure 6d), compared to that formed in the reactor operated in the purely homogeneous combustion mode (Figure 8d). Additionally, the rate of the reaction at atmospheric pressure would be the fastest in the reactor operated in the coupled combustion mode, as illustrated in Figure 14. While heterogeneous pathways that are predominant in the catalytic combustion process occurred in the reactor at elevated temperatures, the contribution to fuel oxidation from homogeneous pathways may be significant, depending on the operating conditions used.

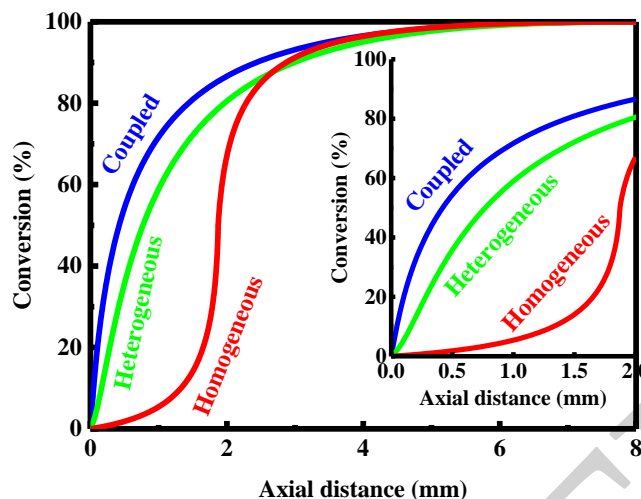


Figure 14. Methane conversion profiles obtained for the reactor described in terms of the coupled combustion mode, the purely heterogeneous combustion mode, and the purely homogeneous combustion mode. All parameters are set to standard values.

The results shown in Figure 12 indicate that conversion of the fuel at high pressures first has an ignition-delay or induction feature, but then it is very similar to that predicted in the reactor described in terms of the purely heterogeneous combustion mode. The rate of overall reaction increases with increasing pressure, but it is inconsistent with that obtained based on pressure squared. Furthermore, the rate of overall reaction is also less than that predicted from the catalytic combustion process described by first-order chemical kinetics. The results shown in Figure 13 also indicate that the formation of the nitrogen oxides in a high temperature environment is favored at high pressures. Therefore, the contribution to the oxidation of the fuel from homogeneous pathways increases with increasing pressure at elevated temperatures, while heterogeneous pathways still predominate the catalytic combustion process that occurred in the reactor.

The effect of pressure on the rate of the combustion reaction in a high temperature environment is a subject worth exploring in depth. The homogeneous reaction occurs in the gas phase essentially via a straight chain process. Gas-phase radical species must accumulate prior to the start of combustion, which leads to an ignition delay for the fuel as shown in Figure 8. The rate-limiting step in the heterogeneous pathway is the dissociation of the fuel molecules on the surface of the catalyst, which is a first-order chemical reaction. Therefore, the rate of the heterogeneous reaction increases almost linearly with pressure. On the other hand, the rate of the homogeneous reaction tends to be proportional to the pressure squared, as stated previously. The ratio of the rate of the homogeneous reaction to that of the heterogeneous reaction increases at roughly the same rate as the pressure, leading to the pressure dependence shown in Figures 12 and 13. Under these conditions, the presence of the catalyst has a significant inhibiting effect on the initiation of homogeneous reactions. The rate of homogeneous reaction increases with increasing pressure, but the initiation of the homogeneous oxidation reaction is greatly inhibited by the heterogeneous reaction, making it possible for the heterogeneous pathway to dominate the catalytic combustion process.

The effect of temperature on the two competing pathways involved is discussed below. Note in particular that the homogeneous reaction in the combustion environment being studied is favored at high temperatures. The results shown in Figure 11 indicate that at wall temperatures below 1400 K, complete conversion of the fuel involved in combustion is impossible under the conditions studied herein, but the rate of the combustion reaction increases with increasing wall temperature. However, conversion of the fuel is similar to that predicted in the reactor operated in the purely heterogeneous combustion mode. The amount of nitric oxide formed during high-temperature combustion increases with increasing wall temperature. Nitric oxide is formed only in the gas phase, but at least a portion of this product is formed during high-temperature combustion through the thermal mechanism, also

known as the extended Zel'dovich mechanism [32]. This thermal route is a secondary mechanism for the formation of nitric oxide since the flame temperatures are relatively low. If flame temperatures are above 1800 K, the thermal route will be a primary mechanism [32]. Therefore, a common approach to control the formation of nitrogen oxides is to reduce the flame temperatures so that very little thermal nitrogen oxides can form in this regard.

The results shown in Figure 8 indicate that in the purely homogenous combustion mode, the concentration peak of the hydroxyl radicals formed within the catalytic reactor appears just after complete conversion of the fuel involved in combustion. The results shown in Figure 6 indicate that in the coupled combustion mode, the peak appears much earlier, with a decrease in peak concentration. The difference in magnitude and position of the peak can be identified most easily by examining the results shown in Figure 10. As the reactor dimension increases, the homogeneous reaction becomes more important due to the decreased surface-area-to-volume ratio associated with larger reactors, and, accordingly, there is a transition of the main reaction pathway. Additionally, the amount of nitrogen oxides formed during high-temperature combustion increases. Furthermore, a large amount of the nitrogen oxides formed in combustion shifts the peak downstream with a large increase in the magnitude of the peak, as shown in Figure 10. Therefore, the formation of nitrogen oxides correlates with the position of the peak, and the contribution to fuel oxidation from homogeneous pathways becomes more important at elevated temperatures.

5.2. Formation and Control of Carbon Monoxide

Catalytic combustion technology can be used to reduce the formation of undesired products [95,96], as discussed early. The results shown in Figure 8 indicate that in the purely homogeneous combustion mode, carbon monoxide is continuously formed from the oxidation of the fuel in the gas phase, until complete conversion of the fuel involved in combustion is achieved within the catalytic reactor, and then this partially oxidized product is converted to carbon dioxide. The results shown in Figure 7 indicate that in the purely heterogeneous combustion mode, carbon monoxide is formed within the catalytic reactor very quickly, but it is easily converted to carbon dioxide. After complete conversion of the fuel involved in combustion, the concentration of this partially oxidized product remains essentially constant. Therefore, in the coupled combustion mode, once complete conversion of the fuel is achieved, the emissions of carbon monoxide will be low. In contrast, in the purely homogeneous combustion mode, the emissions of carbon monoxide are at their peak value just before the homogeneous reaction proceeds to completion. Its peak concentration in the two combustion modes is nearly the same, suggesting a primarily heterogeneous reaction mechanism.

The results shown in Figure 13 indicate that in the combustion environment being studied, the formation of carbon monoxide becomes less favorable at high pressures at which the homogeneous pathway becomes more favorable. At a constant wall temperature of 1500 K, the amount of carbon monoxide formed within the catalytic reactor first decreases slightly and then falls off rapidly with increasing pressure. Any carbon monoxide formed within the catalytic reactor is eventually oxidized into carbon dioxide. An increase in total pressure will shift the equilibrium to the carbon dioxide side, and will reduce the concentration of this partially oxidized product formed in the catalytic reactor, even though the homogeneous reaction becomes more important.

5.3. Formation and Control of the Oxides of Nitrogen

The results presented in the present work indicate that the formation of nitrogen oxides can be significantly reduced by utilizing a catalytic combustion approach under all conditions herein. At temperatures below 1800 K, nitrogen oxides are formed within the catalytic reactor by the prompt mechanism due to the reaction of molecular nitrogen with the radicals such as methylidyne and methylene fragments derived from the fuel being burnt with a catalyst. The prompt mechanism is sometimes referred to as "Fenimore-prompt" or just "Fenimore" [32]. In contrast, at temperatures above 1800 K, they are formed primarily by the well-known thermal mechanism (i.e., the extended

Zel'dovich mechanism), whereas the contribution from the prompt mechanism can be considered to be negligible. To clarify the mechanisms and key elementary reactions for nitrogen oxides formation, numerical simulations are performed for the reactor operated in the coupled combustion mode. The results indicate that the presence of the catalyst can not only greatly reduce the magnitude of gaseous methylidyne and methylene radicals, but also shift their peaks upstream (data not shown). These gaseous species can be oxidized, or further converted to hydrogen cyanide radicals and then isocyanate radicals, and eventually to nitric oxide.

Figure 15 depicts the concentration profiles of the isocyanate and hydrogen cyanide radicals, i.e., the precursors of prompt-nitrogen oxides [97,98], along the direction parallel to the flow. In the combustion environment being studied, both radicals show a peak at the same axial distance as the peak of hydroxyl radicals in the reactor operated in the purely homogeneous combustion mode, as shown in Figure 8. In contrast, there is no concentration peak observed for hydrogen cyanide and isocyanate radicals in the reactor operated in the coupled combustion mode, as shown in Figure 15. As a consequence, prompt-nitrogen oxides are responsible for the formation of nitric oxide in the catalytic reactor operated under the conditions studied herein.

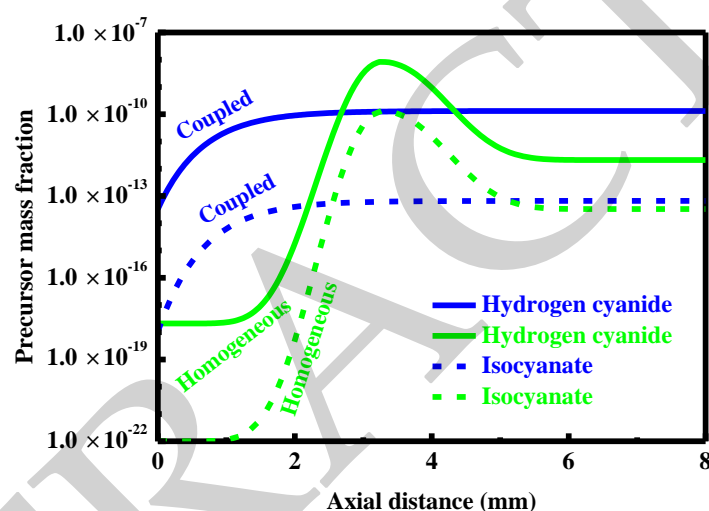


Figure 15. Concentration profiles of the precursors of prompt-nitrogen oxides predicted by the purely homogeneous combustion mode and by the coupled combustion mode, respectively. All parameters are set to standard values.

6. Conclusions

The characteristics of the catalytically-supported thermal combustion of methane diluted in air in small-scale systems were studied at elevated temperatures by using a detailed description of chemical kinetics and molecular transport in order to achieve ultralow pollutant emissions through the control of operating conditions. The effect of various parameters on the performance of the small-scale system was investigated to reduce emissions and improve efficiency, and to determine which factors are of greatest importance in the formation and removal processes of pollutants.

The results indicated that the presence of the catalyst can significantly reduce the emissions of the pollutants formed at elevated temperatures where both heterogeneous and homogeneous reactions can occur simultaneously; however, it is difficult to eliminate these combustion-generated pollutants entirely. Conversion of the fuel to the products of complete combustion has been achieved at very short residence times, without significant production of nitrogen oxides and carbon monoxide. The distribution of catalytically oxidized products depends strongly upon the feed composition, dimension, temperature, and pressure. The interplay between heterogeneous and homogeneous reaction pathways via radicals is strong, which highlights the intrinsic importance of reaction pathways to combustion. Due partly to the adsorption of gas-phase radical species, the presence of the catalyst

significantly inhibits homogeneous reactions, so that the amount of either nitric oxide or carbon monoxide formed during catalytic combustion is negligible at elevated temperatures. Nitric oxide is the main nitrogen pollutant formed during catalytic combustion, with a small amount of nitrogen dioxide. It is necessary to ensure enough selectivity of the catalyst to avoid the formation of gas-phase combustion promoters such as carbon monoxide and nitrogen oxides. The small-scale catalytic system offers the advantages of the ability to support changing operating conditions and of high efficiency with lean fuel-air mixtures.

Catalytic combustion is technically successful, thereby making progress towards small-scale low-emission energy systems. However, the cost and complexity of small-scale catalytic systems may make this technology unattractive for some applications. Further research is required to meet aggressive emission goals while incorporating catalytic combustion technology, and to address the various issues associated with changes in design parameters required for specific applications.

Author Contributions: J.C. designed the simulations, developed the model, analyzed the results, and wrote the paper. X.G. and D.X. assisted in both the analysis of the results and writing of the paper.

Funding: This research was funded by the National Natural Science Foundation of China, grant number No. 51506048.

Acknowledgments: The author thanks the research group of Olaf Deutschmann (Karlsruhe Institute of Technology) for the detailed chemical kinetics of methane oxidation on supported platinum, and the Gas Research Institute for the GRI-Mech combustion model.

Conflicts of Interest: The authors declare no conflict of interest.

References

1. Shirsat, V.; Gupta, A.K. A review of progress in heat recirculating meso-scale combustors. *Appl. Energy* **2011**, *88*, 4294–4309. [[CrossRef](#)]
2. Walther, D.C.; Ahn, J. Advances and challenges in the development of power-generation systems at small scales. *Prog. Energy Combust. Sci.* **2011**, *37*, 583–610. [[CrossRef](#)]
3. Haynes, B.S. Combustion research for chemical processing. *Proc. Combust. Inst.* **2018**, in press. [[CrossRef](#)]
4. Chou, S.K.; Yang, W.M.; Chua, K.J.; Li, J.; Zhang, K.L. Development of micro power generators-A review. *Appl. Energy* **2011**, *88*, 1–16. [[CrossRef](#)]
5. Kaisare, N.S.; Vlachos, D.G. A review on microcombustion: Fundamentals, devices and applications. *Prog. Energy Combust. Sci.* **2012**, *38*, 321–359. [[CrossRef](#)]
6. Ju, Y.; Maruta, K. Microscale combustion: Technology development and fundamental research. *Prog. Energy Combust. Sci.* **2011**, *37*, 669–715. [[CrossRef](#)]
7. Ribeirinha, P.; Abdollahzadeh, M.; Pereira, A.; Relvas, F.; Boaventura, M.; Mendes, A. High temperature PEM fuel cell integrated with a cellular membrane methanol steam reformer: Experimental and modelling. *Appl. Energy* **2018**, *215*, 659–669. [[CrossRef](#)]
8. Chen, Y.; Yao, F.; Huang, X. Mass transfer and reaction in methanol steam reforming reactor with fractal tree-like microchannel network. *Int. J. Heat Mass Transfer* **2015**, *87*, 279–283. [[CrossRef](#)]
9. Engelbrecht, N.; Chiuta, S.; Bessarabov, D.G. A highly efficient autothermal microchannel reactor for ammonia decomposition: Analysis of hydrogen production in transient and steady-state regimes. *J. Power Sources* **2018**, *386*, 47–55. [[CrossRef](#)]
10. Kim, J.H.; Um, D.H.; Kwon, O.C. Hydrogen production from burning and reforming of ammonia in a microreforming system. *Energy Convers. Manage.* **2012**, *56*, 184–191. [[CrossRef](#)]
11. Hockett, A.; Hampson, G.; Marchese, A.J. Development and validation of a reduced chemical kinetic mechanism for computational fluid dynamics simulations of natural gas/diesel dual-fuel engines. *Energy Fuels* **2016**, *30*, 2414–2427. [[CrossRef](#)]
12. Tyagi, A.; Boxx, I.; Peluso, S.; O'Connor, J. The role of flow interaction in flame-flame interaction events in a dual burner experiment. *Proc. Combust. Inst.* **2018**, in press. [[CrossRef](#)]
13. Yehia, O.R.; Reuter, C.B.; Ju, Y. Low-temperature multistage warm diffusion flames. *Combust. Flame* **2018**, *195*, 63–74. [[CrossRef](#)]

14. Burrell, R.R.; Lee, D.J.; Egolfopoulos, F.N. Propagation and extinction of subatmospheric counterflow methane flames. *Combust. Flame* **2018**, *195*, 117–127. [[CrossRef](#)]
15. Smyth, S.A.; Kyritsis, D.C. Experimental determination of the structure of catalytic micro-combustion flows over small-scale flat plates for methane and propane fuel. *Combust. Flame* **2012**, *159*, 802–816. [[CrossRef](#)]
16. Lyubovsky, M.; Smith, L.L.; Castaldi, M.; Karim, H.; Nentwick, B.; Etemad, S.; LaPierre, R.; Pfefferle, W.C. Catalytic combustion over platinum group catalysts: Fuel-lean versus fuel-rich operation. *Catal. Today* **2003**, *83*, 71–84. [[CrossRef](#)]
17. Gancarczyk, A.; Iwaniszyn, M.; Piątek, M.; Korpyś, M.; Sinderka, K.; Jodłowski, P.J.; Łojewska, J.; Kołodziej, A. Catalytic combustion of low-concentration methane on structured catalyst supports. *Ind. Eng. Chem. Res.* **2018**, *57*, 10281–10291. [[CrossRef](#)]
18. Jodłowski, P.J.; Jędrzejczyk, R.J.; Chlebda, D.; Gierada, M.; Łojewska, J. In situ spectroscopic studies of methane catalytic combustion over Co, Ce, and Pd mixed oxides deposited on a steel surface. *J. Catal.* **2017**, *350*, 1–12. [[CrossRef](#)]
19. Nguyen, V.N.; Deja, R.; Peters, R.; Blum, L.; Stolten, D. Study of the catalytic combustion of lean hydrogen-air mixtures in a monolith reactor. *Int. J. Hydrogen Energy* **2018**, *43*, 17520–17530. [[CrossRef](#)]
20. San José, M.J.; Alvarez, S.; López, R. Catalytic combustion of vineyard pruning waste in a conical spouted bed combustor. *Catal. Today* **2018**, *305*, 13–18. [[CrossRef](#)]
21. Carroni, R.; Griffin, T. Catalytic, hybrid lean combustion for gas turbines. *Catal. Today* **2010**, *155*, 2–12. [[CrossRef](#)]
22. Forzatti, P. Status and perspectives of catalytic combustion for gas turbines. *Catal. Today* **2003**, *83*, 3–18. [[CrossRef](#)]
23. Mundhwa, M.; Thurgood, C.P. Numerical study of methane steam reforming and methane combustion over the segmented and continuously coated layers of catalysts in a plate reactor. *Fuel Process. Technol.* **2017**, *158*, 57–72. [[CrossRef](#)]
24. Di Benedetto, A.; Landi, G.; Di Sarli, V.; Barbato, P.S.; Pirone, R.; Russo, G. Methane catalytic combustion under pressure. *Catal. Today* **2012**, *197*, 206–213. [[CrossRef](#)]
25. Richardson, J.T.; Shafiei, M.; Cantu, T.; Machiraju, D.; Telleen, S. Low NO_x emission combustion catalyst using ceramic foam supports. *Stud. Surf. Sci. Catal.* **2004**, *147*, 457–462.
26. D'Alessandro, F.; Pacchiarotta, G.; Rubino, A.; Sperandio, M.; Villa, P.; Carrera, A.M.; Fakhrai, R.; Marra, G.; Congiu, A. Lean catalytic combustion for ultra-low emissions at high temperature in gas-turbine burners. *Energy Fuels* **2011**, *25*, 136–143. [[CrossRef](#)]
27. Runyon, J.; Marsh, R.; Bowen, P.; Pugh, D.; Giles, A.; Morris, S. Lean methane flame stability in a premixed generic swirl burner: Isothermal flow and atmospheric combustion characterization. *Exp. Therm. Fluid Sci.* **2018**, *92*, 125–140. [[CrossRef](#)]
28. Jainski, C.; Reißmann, M.; Böhm, B.; Janicka, J.; Dreizler, A. Sidewall quenching of atmospheric laminar premixed flames studied by laser-based diagnostics. *Combust. Flame* **2017**, *183*, 271–282. [[CrossRef](#)]
29. James, A.; Brindley, J.; McIntosh, A.C. Classification of behaviour in a steady plug-flow model of catalytic combustion. *Chem. Eng. Sci.* **2001**, *56*, 4649–4658. [[CrossRef](#)]
30. James, A.; Brindley, J.; McIntosh, A.C. Stability of multiple steady states of catalytic combustion. *Combust. Flame* **2002**, *130*, 137–146. [[CrossRef](#)]
31. Tolmachoff, E.D.; Booth, A.D.; Lee, I.C.; Allmon, W.R.; Waits, C.M. Modeling and experimental analysis of n-dodecane oxidation in platinum-coated channels. *Combust. Flame* **2015**, *162*, 3674–3680. [[CrossRef](#)]
32. Richards, G.A.; McMillian, M.M.; Gemmen, R.S.; Rogers, W.A.; Cully, S.R. Issues for low-emission, fuel-flexible power systems. *Prog. Energy Combust. Sci.* **2001**, *27*, 141–169. [[CrossRef](#)]
33. Li, Y.-H.; Chen, G.-B.; Wu, F.-H.; Cheng, T.-S.; Chao, Y.-C. Combustion characteristics in a small-scale reactor with catalyst segmentation and cavities. *Proc. Combust. Inst.* **2013**, *34*, 2253–2259. [[CrossRef](#)]
34. Li, Y.-H.; Chen, G.-B.; Wu, F.-H.; Cheng, T.-S.; Chao, Y.-C. Effects of catalyst segmentation with cavities on combustion enhancement of blended fuels in a micro channel. *Combust. Flame* **2012**, *159*, 1644–1651. [[CrossRef](#)]
35. Shimizu, T.; Abid, A.D.; Poskrebyshev, G.; Wang, H.; Nabity, J.; Engel, J.; Yu, J.; Wickham, D.; Van Devener, B.; Anderson, S.L.; Williams, S. Methane ignition catalyzed by in situ generated palladium nanoparticles. *Combust. Flame* **2010**, *157*, 421–435. [[CrossRef](#)]

36. Kommu, M.; Kaisare, N.S. Ignition of homo/hetero combustion of propane in a microreactor with catalyst segmentation. *Chem. Eng. Res. Des.* **2018**, *138*, 125–134. [[CrossRef](#)]
37. Jeon, S.W.; Yoon, W.J.; Jeong, M.W.; Kim, Y. Optimization of a counter-flow microchannel reactor using hydrogen assisted catalytic combustion for steam reforming of methane. *Int. J. Hydrogen Energy* **2014**, *39*, 6470–6478. [[CrossRef](#)]
38. Mundhwa, M.; Parmar, R.D.; Thurgood, C.P. A comparative parametric study of a catalytic plate methane reformer coated with segmented and continuous layers of combustion catalyst for hydrogen production. *J. Power Sources* **2017**, *344*, 85–102. [[CrossRef](#)]
39. Kunte, A.; Raghu, A.K.; Kaisare, N.S. A spiral microreactor for improved stability and performance for catalytic combustion of propane. *Chem. Eng. Sci.* **2018**, *187*, 87–97. [[CrossRef](#)]
40. Carroni, R.; Griffin, T.; Kelsall, G. Cathlean: catalytic, hybrid, lean-premixed burner for gas turbines. *Appl. Therm. Eng.* **2004**, *24*, 1665–1676. [[CrossRef](#)]
41. Kaisare, N.S.; Deshmukh, S.R.; Vlachos, D.G. Stability and performance of catalytic microreactors: Simulations of propane catalytic combustion on Pt. *Chem. Eng. Sci.* **2008**, *63*, 1098–1116. [[CrossRef](#)]
42. Goralski, C.T.; Schmidt, L.D. Modeling heterogeneous and homogeneous reactions in the high-temperature catalytic combustion of methane. *Chem. Eng. Sci.* **1999**, *54*, 5791–5807. [[CrossRef](#)]
43. Fumey, B.; Buetler, T.; Vogt, U.F. Ultra-low NO_x emissions from catalytic hydrogen combustion. *Appl. Energy* **2018**, *213*, 334–342. [[CrossRef](#)]
44. Hinokuma, S.; Kiritoshi, S.; Kawabata, Y.; Araki, K.; Matsuki, S.; Sato, T.; Machida, M. Catalytic ammonia combustion properties and operando characterization of copper oxides supported on aluminum silicates and silicon oxides. *J. Catal.* **2018**, *361*, 267–277. [[CrossRef](#)]
45. Pfefferle, L.D. Heterogeneous/homogeneous reactions and transport coupling for catalytic combustion systems: a review of model alternatives. *Catal. Today* **1995**, *26*, 255–265. [[CrossRef](#)]
46. Westbrook, C.K.; Mizobuchi, Y.; Poinso, T.J.; Smith, P.J.; Warnatz, J. Computational combustion. *Proc. Combust. Inst.* **2005**, *30*, 125–157. [[CrossRef](#)]
47. Law, C.K. Combustion at a crossroads: Status and prospects. *Proc. Combust. Inst.* **2007**, *31*, 1–29. [[CrossRef](#)]
48. Miller, J.A.; Pilling, M.J.; Troe, J. Unravelling combustion mechanisms through a quantitative understanding of elementary reactions. *Proc. Combust. Inst.* **2005**, *301*, 43–88. [[CrossRef](#)]
49. Klippenstein, S.J. From theoretical reaction dynamics to chemical modeling of combustion. *Proc. Combust. Inst.* **2017**, *36*, 77–111. [[CrossRef](#)]
50. Buckmaster, J.; Clavin, P.; Liñán, A.; Matalon, M.; Peters, N.; Sivashinsky, G.; Williams, F.A. Combustion theory and modeling. *Proc. Combust. Inst.* **2005**, *30*, 1–19. [[CrossRef](#)]
51. Kiefer, J.; Ewart, P. Laser diagnostics and minor species detection in combustion using resonant four-wave mixing. *Prog. Energy Combust. Sci.* **2011**, *37*, 525–564. [[CrossRef](#)]
52. Michelsen, H.A.; Schulz, C.; Smallwood, G.J.; Will, S. Laser-induced incandescence: Particulate diagnostics for combustion, atmospheric, and industrial applications. *Prog. Energy Combust. Sci.* **2015**, *51*, 2–48. [[CrossRef](#)]
53. Choudary, C.; Mazumder, S. Direct numerical simulation of catalytic combustion in a multi-channel monolith reactor using personal computers with emerging architectures. *Comput. Chem. Eng.* **2014**, *61*, 175–184. [[CrossRef](#)]
54. Curran, H.J. Developing detailed chemical kinetic mechanisms for fuel combustion. *Proc. Combust. Inst.* **2018**, in press. [[CrossRef](#)]
55. Deutschmann, O.; Maier, L.I.; Riedel, U.; Stroemman, A.H.; Dibble, R.W. Hydrogen assisted catalytic combustion of methane on platinum. *Catal. Today* **2000**, *59*, 141–150. [[CrossRef](#)]
56. Williams, J.L. Monolith structures, materials, properties and uses. *Catal. Today* **2001**, *69*, 3–9. [[CrossRef](#)]
57. Nijhuis, T.A.; Beers, A.E.W.; Vergunst, T.; Hoek, I.; Kapteijn, F.; Moulijn, J.A. Preparation of monolithic catalysts. *Catal. Rev.* **2001**, *43*, 345–380. [[CrossRef](#)]
58. Fichtner, M.; Mayer, J.; Wolf, D.; Schubert, K. Microstructured rhodium catalysts for the partial oxidation of methane to syngas under pressure. *Ind. Eng. Chem. Res.* **2001**, *40*, 3475–3483. [[CrossRef](#)]
59. Tornaiainen, P.M.; Chu, X.; Schmidt, L.D. Comparison of monolith-supported metals for the direct oxidation of methane to syngas. *J. Catal.* **1994**, *146*, 1–10. [[CrossRef](#)]
60. Deshmukh, S.R.; Vlachos, D.G. Effect of flow configuration on the operation of coupled combustor/reformer microdevices for hydrogen production. *Chem. Eng. Sci.* **2005**, *60*, 5718–5728. [[CrossRef](#)]

61. Stefanidis, G.D.; Vlachos, D.G. Intensification of steam reforming of natural gas: Choosing combustible fuel and reforming catalyst. *Chem. Eng. Sci.* **2010**, *65*, 398–404. [[CrossRef](#)]
62. Deshmukh, S.R.; Vlachos, D.G. CFD simulations of coupled, countercurrent combustor/reformer microdevices for hydrogen production. *Ind. Eng. Chem. Res.* **2005**, *44*, 4982–4992. [[CrossRef](#)]
63. Stefanidis, G.D.; Kaisare, N.S.; Vlachos, D.G. Modeling ignition in catalytic microreactors. *Chem. Eng. Technol.* **2008**, *31*, 1170–1175. [[CrossRef](#)]
64. Miller, J.A.; Bowman, C.T. Mechanism and modeling of nitrogen chemistry in combustion. *Prog. Energy Combust. Sci.* **1989**, *15*, 287–338. [[CrossRef](#)]
65. Hill, S.C.; Douglas Smoot, L. Modeling of nitrogen oxides formation and destruction in combustion systems. *Prog. Energy Combust. Sci.* **2000**, *26*, 417–458. [[CrossRef](#)]
66. Lipatnikov, A.N. Stratified turbulent flames: Recent advances in understanding the influence of mixture inhomogeneities on premixed combustion and modeling challenges. *Prog. Energy Combust. Sci.* **2017**, *62*, 87–132. [[CrossRef](#)]
67. van Oijen, J.A.; Donini, A.; Bastiaans, R.J.M.; ten Thije Boonkkamp, J.H.M.; de Goey, L.P.H. State-of-the-art in premixed combustion modeling using flamelet generated manifolds. *Prog. Energy Combust. Sci.* **2016**, *57*, 30–74. [[CrossRef](#)]
68. *ANSYS Fluent User's Guide*; Release 16.0; ANSYS Inc.: Canonsburg, PA, USA, 2014.
69. Versteeg, H.K.; Malalasekera, W. *An Introduction to Computational Fluid Dynamics: The Finite Volume Method Approach, Second Edition*; Pearson Education Limited: London, UK, 2007.
70. Blasi, J.M.; Weddle, P.J.; Karakaya, C.; Diercks, D.R.; Kee, R.J. Modeling reaction-diffusion processes within catalyst washcoats: II. Macroscale processes informed by microscale simulations. *Chem. Eng. Sci.* **2016**, *145*, 308–316. [[CrossRef](#)]
71. Bidabehere, C.M.; García, J.R.; Sedran, U. Transient effectiveness factors in the dynamic analysis of heterogeneous reactors with porous catalyst particles. *Chem. Eng. Sci.* **2015**, *137*, 293–300. [[CrossRef](#)]
72. Gonzalez-Juez, E.D.; Kerstein, A.R.; Ranjan, R.; Menon, S. Advances and challenges in modeling high-speed turbulent combustion in propulsion systems. *Prog. Energy Combust. Sci.* **2017**, *60*, 26–67. [[CrossRef](#)]
73. Dogwiler, U.; Benz, P.; Mantzaras, J. Two-dimensional modelling for catalytically stabilized combustion of a lean methane-air mixture with elementary homogeneous and heterogeneous chemical reactions. *Combust. Flame* **1999**, *116*, 243–258. [[CrossRef](#)]
74. Smith, G.P.; Golden, D.M.; Frenklach, M.; Moriarty, N.W.; Eiteneer, B.; Goldenberg, M.; Bowman, C.T.; Hanson, R.K.; Song, S.; Gardiner, W.C., Jr.; et al. *GRI-Mech Version 3.0*; Gas Research Institute: Chicago, IL, USA, 2000.
75. Simmie, J.M. Detailed chemical kinetic models for the combustion of hydrocarbon fuels. *Prog. Energy Combust. Sci.* **2003**, *29*, 599–634. [[CrossRef](#)]
76. Kee, R.J.; Rupley, F.M.; Meeks, E.; Miller, J.A. *CHEMKIN-III: A Fortran Chemical Kinetics Package for the Analysis of Gasphase Chemical and Plasma Kinetics*; Report No. SAND96-8216; Sandia National Laboratories: Livermore, CA, USA, 1996.
77. Coltrin, M.E.; Kee, R.J.; Rupley, F.M.; Meeks, E. *SURFACE CHEMKIN-III: A Fortran package for analyzing heterogeneous chemical kinetics at a solid-surface-gas-phase interface*; Report No. SAND96-8217; Sandia National Laboratories: Livermore, CA, USA, 1996.
78. Dogwiler, U.; Mantzaras, J.; Benz, P.; Kaeppli, B.; Bombach, R.; Arnold, A. Homogeneous ignition of methane-air mixtures over platinum: Comparison of measurements and detailed numerical predictions. *Symp. (Int.) Comb.* **1998**, *27*, 2275–2282. [[CrossRef](#)]
79. Bensalem, O.; Ernst, W.R. Mathematical modeling of homogeneous-heterogeneous reactions in monolithic catalyst. *Combust. Sci. Technol.* **1982**, *29*, 1–13. [[CrossRef](#)]
80. Alam, I.; West, D.H.; Balakotaiah, V. Transport effects on pattern formation and maximum temperature in homogeneous-heterogeneous combustion. *Chem. Eng. J.* **2016**, *288*, 99–115. [[CrossRef](#)]
81. Harrison, B.K.; Ernst, W.R. Catalytic combustion in cylindrical channels: a homogeneous-heterogeneous model. *Combust. Sci. Technol.* **1978**, *19*, 31–38. [[CrossRef](#)]
82. Chattopadhyay, S.; Veser, G. Heterogeneous-homogeneous interactions in catalytic microchannel reactors. *AIChE J.* **2006**, *52*, 2217–2229. [[CrossRef](#)]
83. Bucci, M.A.; Robinet, J.-C.; Chibbaro, S. Global stability analysis of 3D micro-combustion model. *Combust. Flame* **2016**, *167*, 132–148. [[CrossRef](#)]

84. Gauthier, G.P.; Bergthorson, J.M. Effect of external heat loss on the propagation and quenching of flames in small heat-recirculating tubes. *Combust. Flame* **2016**, *173*, 27–38. [[CrossRef](#)]
85. Pfefferle, W.C.; Pfefferle, L.D. Catalytically stabilized combustion. *Prog. Energy Combust. Sci.* **1986**, *12*, 25–41. [[CrossRef](#)]
86. Kohse-Höinghaus, K. Clean combustion: Chemistry and diagnostics for a systems approach in transportation and energy conversion. *Prog. Energy Combust. Sci.* **2018**, *65*, 1–5. [[CrossRef](#)]
87. Hansen, N.; Cool, T.A.; Westmoreland, P.R.; Kohse-Höinghaus, K. Recent contributions of flame-sampling molecular-beam mass spectrometry to a fundamental understanding of combustion chemistry. *Prog. Energy Combust. Sci.* **2009**, *35*, 168–191. [[CrossRef](#)]
88. Egolfopoulos, F.N.; Hansen, N.; Ju, Y.; Kohse-Höinghaus, K.; Law, C.K.; Qi, F. Advances and challenges in laminar flame experiments and implications for combustion chemistry. *Prog. Energy Combust. Sci.* **2014**, *43*, 36–67. [[CrossRef](#)]
89. Kaisare, N.S.; Vlachos, D.G. Optimal reactor dimensions for homogeneous combustion in small channels. *Catal. Today* **2007**, *120*, 96–106. [[CrossRef](#)]
90. Miesse, C.M.; Masel, R.I.; Jensen, C.D.; Shannon, M.A.; Short, M. Submillimeter-scale combustion. *AIChE J.* **2004**, *50*, 3206–3214. [[CrossRef](#)]
91. Carriere, T.; Westmoreland, P.R.; Kazakov, A.; Stein, Y.S.; Dryer, F.L. Modeling ethylene combustion from low to high pressure. *Proc. Combust. Inst.* **2002**, *29*, 1257–1266. [[CrossRef](#)]
92. Madane, K.; Kulkarni, A.A. Pressure equalization approach for flow uniformity in microreactor with parallel channels. *Chem. Eng. Sci.* **2018**, *176*, 96–106. [[CrossRef](#)]
93. Hunt, G.; Karimi, N.; Torabi, M. Two-dimensional analytical investigation of coupled heat and mass transfer and entropy generation in a porous, catalytic microreactor. *Int. J. Heat Mass Transfer* **2018**, *119*, 372–391. [[CrossRef](#)]
94. Sattari-Najafabadi, M.; Nasr Esfahany, M.; Wu, Z.; Sunden, B. Mass transfer between phases in microchannels: A review. *Chem. Eng. Process. Process Intensif.* **2018**, *127*, 213–237. [[CrossRef](#)]
95. Basini, L. Fuel rich catalytic combustion: Principles and technological developments in short contact time (SCT) catalytic processes. *Catal. Today* **2006**, *117*, 384–393. [[CrossRef](#)]
96. Choudhary, T.V.; Banerjee, S.; Choudhary, V.R. Catalysts for combustion of methane and lower alkanes. *Appl. Catal. A* **2002**, *234*, 1–23. [[CrossRef](#)]
97. Glarborg, P.; Miller, J.A.; Ruscic, B.; Klippenstein, S.J. Modeling nitrogen chemistry in combustion. *Prog. Energy Combust. Sci.* **2018**, *67*, 31–68. [[CrossRef](#)]
98. Hashemi, H.; Jacobsen, J.G.; Rasmussen, C.T.; Christensen, J.M.; Glarborg, P.; Gersen, S.; van Essen, M.; Levinsky, H.B.; Klippenstein, S.J. High-pressure oxidation of ethane. *Combust. Flame* **2017**, *182*, 150–166. [[CrossRef](#)]



© 2018 by the authors. Licensee MDPI, Basel, Switzerland. This article is an open access article distributed under the terms and conditions of the Creative Commons Attribution (CC BY) license (<http://creativecommons.org/licenses/by/4.0/>).